CO_2-Enhanced Diffusion of Azobenzene in Glassy Polystyrene near the Glass Transition

B. R. Chapman,[†] C. R. Gochanour,[‡] and M. E. Paulaitis*[,†,§]

Center for Molecular and Engineering Thermodynamics, Department of Chemical Engineering, University of Delaware, Newark, Delaware 19716, and Central Research and Development Department, Experimental Station, E. I. du Pont de Nemours and Company, Wilmington, Delaware 19880

Received September 28, 1995; Revised Manuscript Received May 21, 1996[⊗]

ABSTRACT: Forced Rayleigh scattering (FRS) has been used to measure the tracer diffusion coefficient of azobenzene in low molecular weight polystyrene (PS) as a function of temperature, and in high molecular weight PS plasticized by CO_2 at 35 °C and CO_2 pressures from 14 to 85 bar. In contrast to dye diffusion in pure PS and PS plasticized by tricresyl phosphate, where the effect of plasticization by temperature, chain ends, or added diluent can be accounted for by $(T - T_g)$ scaling, dye diffusion in CO_2-plasticized PS is enhanced by 2−3 orders of magnitude over values predicted on the basis of T_g depression alone. This enhancement begins at surprisingly low CO_2 pressures (<15 bar at 35 °C) and is maintained across the CO_2-induced glass transition. A large difference in mobilities of the *cis* and *trans* isomers of azobenzene is also observed in the presence of CO_2, which is much greater than that seen in the experiments on pure PS. Two additional FRS relaxation modes unrelated to translational diffusion of the dye molecules have been identified in this study: a fast, local relaxation attributed to dye rotation, and a slow relaxation attributed to the dynamic response of the PS/CO_2 matrix to a chemical potential driving force associated with the azobenzene isomers.

I. Introduction

Compressed gases and supercritical fluids are effective plasticizers and mass transfer agents in a number of novel polymer processing applications. Foremost among these is the supercritical fluid (SCF) extraction of low molecular weight materials from polymer matrices[1,2]—for example, residual monomers and solvents,[3] oligomers,[4] and additives[5] from synthetic polymers; and natural products from biological polymeric substrates.[6] Alternatively, SCFs have been used to impregnate polymers with plasticizers and other property modifiers,[7] pharmaceuticals,[8] or organometallic compounds.[9] Similar mass transfer processes also occur during heterogeneous polymerizations in SCF solvents,[10,11] and should play a role in determining final polymer properties by mediating the distribution of monomer, initiator, and chain transfer agent between the polymer-rich and dense fluid phases.

Advantages typically attributed to SCFs in these applications are derived from their unique solvent properties.[1,2] For example, large solubility enhancements and high compressibilities in the near-critical region can be readily exploited to manipulate the equilibrium partitioning of solute between the fluid phase and the polymer matrix simply by adjusting temperature and/or pressure.[12] Mass transfer in the fluid phase is also enhanced in SCFs relative to liquid solvents due to a favorable combination of physical properties, namely a liquid-like density, gas-like viscosity, and high solute diffusivities.[13] However, the overall mass transfer in polymer/SCF systems is likely to be rate-limiting in the polymer-rich phase,[2] making solute diffusivity in this phase a critical parameter in characterizing mass transport in these systems.

As a consequence, it is anticipated that diffusion through a polymer matrix will be strongly affected by the presence of a compressed gas or SCF. This follows not only because mass transfer characteristics of the pure fluid will be reflected to a certain extent in the polymer-rich phase, but from changes induced in the morphology and dynamics of the polymer as well. For example, exposing an amorphous polymer to CO_2 at supercritical temperatures and elevated pressures can result in considerable swelling and plasticization, due to high CO_2 solubilities.[14−22] How such changes might influence solute diffusion in the polymer is not directly evident, but a reasonable expectation is that solute mobility will be significantly enhanced. Also, the magnitude of this enhancement will undoubtedly be a complex function of temperature and pressure, as well as the chemical nature of the SCF.

Quantitative studies of solute mass transfer enhancement in a polymer plasticized by a compressed gas or SCF are scarce. Berens *et al.*[7] first showed that the kinetically-limited incorporation of a solute into a glassy polymer matrix is accelerated by plasticization due to sorbed CO_2. The solute could be effectively trapped in the matrix by dropping CO_2 pressure, allowing rapid removal of the small CO_2 molecules but severely inhibiting diffusion of the larger solute molecules in the unswollen glass. Based on measurements of mass uptake kinetics, solute diffusivity in the polymer was estimated to increase by at least 6 orders of magnitude in the presence of CO_2 at subcritical pressures.[7] A similar enhancement in diffusivity was found by Dooley *et al.*[23] in the extraction of ethylbenzene from polystyrene using supercritical CO_2, while Cotton *et al.*[24] noted enhancements of 2−3 orders of magnitude for the diffusivity of additives in semi-crystalline polypropylene in the presence of supercritical CO_2. Finally, Nealey *et al.*[25] showed that the diffusivity of a much larger solute (polybutadiene oligomer) in polystyrene could be increased by nearly a factor of 10 at a temperature only slightly above T_g via plasticization with compressed argon. In all these studies, solute diffusivities were obtained only indirectly by fitting experimental data to macroscopic transport models of the impregnation or

[†] University of Delaware.
[‡] E. I. du Pont de Nemours and Co.
[§] Present address: Department of Chemical Engineering, Johns Hopkins University, Baltimore, MD 21218.
[⊗] Abstract published in *Advance ACS Abstracts,* July 1, 1996.

S0024-9297(95)01469-0 CCC: $12.00

extraction process, in which the coupling of CO_2 equilibration to the measured kinetics was neglected.

In this work, we report the direct measurement of the diffusivity of a monomer-sized solute in an amorphous, glassy polymer in equilibrium with compressed CO_2 at elevated pressures. Specifically, we have measured the tracer-diffusion coefficients of the *cis* and *trans* isomers of azobenzene in polystyrene as a function of CO_2 pressure at 35 °C using the forced Rayleigh scattering (FRS) technique. The range of pressures studied include that required to lower the glass transition temperature to 35 °C, thereby allowing azobenzene diffusivities to be obtained across the CO_2-induced glass transition.

II. FRS Technique

FRS measures the diffusivity of a photoactive dye molecule in a background matrix by monitoring the rate of relaxation of a "forced" gradient in dye concentration. Since the dye is present at sufficiently low concentrations, it acts as an infinitely dilute probe, and a tracer-diffusion coefficient is obtained. Previous studies of polymer solutions[26] and bulk polymers[27] have demonstrated the broad applicability of FRS to study small-molecule diffusion in polymer systems. The range of accessible diffusion coefficients ($\sim 10^{-5}-10^{-16}$ cm^2/s) covers much of the range of diffusivities encountered in solutions, melts, and glasses, making the technique particularly well suited to study diffusion across the glass transition. This large measurement window is derived from an advantageous combination of the length scale for diffusion (typically 0.5−50 μm) and the time scale for experiments (typically milliseconds to days). We present here a brief description of the basic theory and methodology of FRS; more comprehensive reviews are given elsewhere.[28−31]

The FRS experiment involves two elementary steps: *writing*, which establishes the dye concentration gradient, and *reading*, in which the time evolution of that concentration gradient is measured. During the writing process, a sinusoidal light intensity interference pattern is temporarily established in the sample by crossing two mutually coherent laser beams. The spatial period of this interference pattern, d, is determined by the crossing angle between the beams, θ, and the laser wavelength, λ: $d = \lambda/(2 \sin(\theta/2))$. Dye molecules in the exposed volume undergo a photoreaction, most often an isomerization, to produce a photoproduct from the thermodynamically stable form of the dye originally present uniformly throughout the sample. Since the extent of this photoreaction depends on the intensity of the excitation light, two concentration profiles are created (one for each dye isomer) that mimic the periodicity of the light intensity interference pattern.

Thus, following the writing pulse, two sinusoidal dye concentration gradients (gratings) exist in the sample, characterized by a known period, d, and an amplitude, Δc_0, determined by the maximum extent of photoreaction. These gratings, which are necessarily 180° out of phase, subsequently relax at independent rates as the dye molecules diffuse due to thermal motion. For Fickian diffusion, the spatial distribution of each isomer concentration grating remains sinusoidal, while the amplitude Δc_i decays exponentially in time:

$$\Delta c_i(t) = \Delta c_0 \, e^{-q^2 D_i t} \qquad (1)$$

where q, the magnitude of the grating wave vector, is related to the spatial period ($q = 2\pi/d$), and D_i is the tracer-diffusion coefficient of isomer i. If the lifetime of the photoproduct is comparable to the time scale for diffusion, thermal reconversion back to the stable-state isomer also contributes to the relaxation of the photoproduct concentration gradient. The expression for $\Delta c_i(t)$ then becomes more complicated.[32,33]

The reading process relies on a difference in the refractive index and/or absorption coefficient of the two dye isomers to measure the time dependence of $\Delta c_i(t)$. This difference is manifested in different contributions to the optical properties of the composite system, which are proportional to dye concentration in the low-concentration limit. Consequently, the periodic concentration profiles established by the writing pulse lead to corresponding periodic profiles in optical properties, constituting an optical diffraction grating. The amplitude of such a grating can be probed using a nonexciting laser beam (the reading beam) directed at the Bragg angle, as the intensity of diffracted light and the amplitude are simply related; for example, $I_d \sim (\Delta n)^2$ in the thick grating limit,[34] where Δn represents the amplitude of the refractive index modulation. Thus, the intensity of light diffracted from the reading beam will decay as the amplitude of the optical grating decays. Since the rate of decay is determined by diffusion of the dye molecules (as well as thermal reconversion if it occurs), dye diffusivities are obtained directly from the temporal behavior of the diffracted intensity.

In the most general case, *both* isomer concentration gratings contribute to the optical grating. The time dependence of the diffracted signal intensity is then expressed in the following form:[26,32,33,35−37]

$$I_d = \{A_1 \, e^{-t/\tau_1} - A_2 \, e^{-t/\tau_2} + C_{coh}\}^2 + C_{inc}^2 \qquad (2)$$

where

$$1/\tau_1 = q^2 D_1 \quad \text{and} \quad 1/\tau_2 = q^2 D_2 + 1/\tau_r \qquad (3)$$

This description is commonly referred to as the "dual grating" or "complementary grating" model. Subscripts 1 and 2 refer to the stable-state and photoproduct isomers of the dye, respectively, and each exponential term represents the amplitude of the diffracted optical field from the associated isomer concentration grating. The negative sign between terms reflects the 180° phase difference between these diffracted optical fields. The pre-exponential factor A_i depends on experimental parameters associated with the Bragg diffraction process, physical properties of isomer i and the background matrix, and Δc_0. τ_i is the characteristic time for relaxation of the concentration grating associated with isomer i, and τ_r is the reconversion time for the thermally driven isomerization back-reaction (only the photoproduct undergoes this reaction). C_{coh} and C_{inc} are small coherent and incoherent scattering contributions, respectively. The ratio A_1/A_2 describes the relative diffraction efficiency and depends only on the optical contrast between each isomer and the matrix if thermal reconversion can be neglected (otherwise, it also depends on τ_1, τ_2, and τ_r[32,33]). In all cases, D_i is determined from the slope of a linear plot of $1/\tau_i$ *vs* q^2.

A single-exponential decay results if the isomer diffusivities are identical or if the diffracted optical field from one isomer grating completely dominates the other.

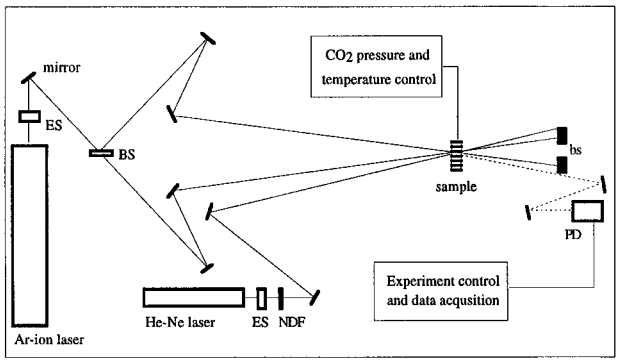

Figure 1. Schematic diagram of the FRS apparatus: BS = beamsplitter, bs = beam stop, NDF = neutral-density filter, PD = photodiode detector, ES = electronic shutter.

However, while isomer diffusivities are often similar, they are usually not identical due to differences in molecular size and shape or interactions with the matrix, and hence the two relaxation times will generally differ. Also, when neither isomer contribution can be neglected, the diffracted optical fields will interfere with one another, either constructively ($A_1/A_2 < 0$) or destructively ($A_1/A_2 > 0$). The result is a nonexponential time dependence for relaxation of the total diffracted optical field, described by eq 2. In fact, under certain conditions for destructive interference, this equation predicts that the measured FRS signal will decay *nonmonotonically*.[26]

III. Experimental Section

A schematic diagram of our FRS apparatus as it is arranged on a vibration-isolation table is shown in Figure 1. The writing laser is a polarized CW argon ion laser (Lexel) tuned to either 488.0 or 514.5 nm. Using a plate beamsplitter, the initial beam is split into two beams of nearly equal intensity that are redirected by mirrors to cross within the sample volume. An etalon in the laser cavity increases the coherence length of the beams well beyond any difference in path length after the split. The crossing angle is established by manually adjusting the positions of the mirrors to direct the beams through pinholes in custom-made alignment jigs. The present setup allows grating spacings of approximately 0.45−12 μm, with an estimated uncertainty of <1% over this entire range. An electronic shutter controls the duration of the writing pulse. For these experiments, writing times of 20−250 ms and intensities of 50−250 mW were employed.

The reading beam from a polarized 10 mW, 632.8 nm He−Ne laser (Melles-Griot) is directed into the sample volume at an angle that satisfies the Bragg condition for the established grating spacing. Alignment again is performed by manually positioning the mirrors to guide the beam through appropriate pinholes in the alignment jigs. The diffracted intensity is detected with a properly aligned silicon photodiode detector (Hamamatsu). An electronic shutter controls the exposure time for the reading beam, while neutral-density filters reduce the initial beam intensity to a value of 1 mW or less. An iris diaphragm and 632.8 ± 3 nm band-pass filter placed in front of the detector minimize the contributions from stray light and the writing beam.

A data acquisition board (National Instruments) in a Macintosh computer controls the timing of the experiment, digitizes the photodiode voltage output, and stores the diffracted intensity *vs* time signal. The uncertainty in the data acquisition timing is ±1 ms, the resolution of the on-board timer; the uncertainty in the digitized signal is <0.1% of the measured value, the precision of 12 bit A/D conversion with a variable gain. When studying diffusion processes over periods of several minutes or longer, the reading beam is shuttered into 50 ms pulses for each data point to minimize possible effects associated with prolonged exposure of the sample to the He−Ne beam. A digital delay/pulse generator (Stanford Research) controls this timing process by precisely sequencing the writing and reading shutters and triggering the data acquisition. This arrangement was used for data acquisition frequencies up to 1 Hz. At higher frequencies, the reading beam remains on continuously while collecting data. In either case, typical runs consist of 500−1500 data points.

The custom-built, high-pressure optical cell is constructed of a stainless steel body, sapphire windows, and Teflon seals, and was tested under hydrostatic pressure to 300 bar. The internal volume of the cell is a cylindrical gap between the windows, 2 mm thick and 1.27 cm in diameter. A Delrin retaining ring is placed around the circumference of this volume to keep the polymer sample pressed against the front window. Compressed gas is introduced through a single port in the cell from a pressure reservoir, which is either a pressure-regulated gas cylinder for pressures less than 68 bar or a CO_2-filled syringe pump for higher pressures. The sample volume can be evacuated through the same port using a mechanical vacuum pump. The cell is housed in a stainless steel jacket which is temperature controlled with a circulating fluid from a constant-temperature bath. The temperature at the outer edge of the cell is monitored using a thermocouple accurate to ±0.5 °C and found to be within ±0.2 °C of that measured inside the cell. We estimate the uncertainty in reported temperatures to be <1 °C and the stability to be ±0.2 °C over the course of an experiment. The pressure in the cell is measured to ±2 psia (±0.1 bar) with a pressure transducer calibrated against dead-weight standards. Daily fluctuations in room temperature have a noticeable effect on the gas pressure in the cylinder or syringe pump, leading to a worst-case pressure stability of ±5 psia (±0.3 bar) over the course of an extended experiment.

The photoreaction for the photochromic dye, azobenzene, is a thermally reversible *trans* to *cis* isomerization, characteristic of azo dyes.[38] Although neither isomer absorbs strongly at the reading wavelength, both isomers make nonnegligible contributions to the net refractive index of the sample. FRS signals from azobenzene and other azodyes have been observed to exhibit nonexponential, nonmonotonic decays in a variety of systems,[26,39,40] indicating a measurable difference in isomer mobilities. For azobenzene, the signals commonly follow "decay−growth−decay" kinetics, described by eq 2 when $A_1 > A_2$ and $\tau_1 < \tau_2$. The thermal reconversion rate for azobenzene is known to be extremely slow: in both polar and nonpolar solvents at room temperature, the lifetime of the *cis* isomer is typically measured in days.[41] While the dye photochemistry and reconversion kinetics are likely to be modified in a concentrated polymer matrix,[42] it has been shown that the *cis* isomer lifetime increases as the matrix viscosity increases in a manner that correlates with the concurrent decrease in diffusivity.[26] Thus, for the experimental time scales studied here, the influence of thermal reconversion on the signal decay, relative to that of diffusion, is expected to be small. This assumption breaks down when diffusion becomes very slow. In fact, the rate of thermal reconversion sets a lower bound on the range of diffusion coefficients that can be measured with our apparatus for this system ($\sim 10^{-15}$ cm^2/s).

Two polystyrenes (Polysciences) were used in this study: a high molecular weight standard, with M_p = 35 800 and M_w/M_n = 1.11 (determined by GPC), hereafter referred to as PS-36K; and an oligomer molecular weight standard, with M_p = 1060 (~10 monomers per chain) and M_w/M_n = 1.11, referred to as PS-1K. Glass transition temperatures, determined by DSC (10 °C/min heating rate, midpoint convention), were 98 ± 2 °C for PS-36K and 15 ± 2 °C for PS-1K. Only PS-36K was used for the CO_2 plasticization experiments. Azobenzene (Kodak) was purified once by sublimation. Carbon dioxide (Matheson, 99.99% purity) was used as received.

The FRS experiment requires a homogeneous, optically transparent sample. Homogeneity of azobenzene in PS-36K was obtained by freeze-drying dilute 1,4-dioxane solutions containing the polymer and dye. Resulting dye concentrations in the solvent-free polymer were 0.2−0.3 wt %, and measured glass transition temperatures were unchanged from the value for pure polymer. Although we have not systematically varied

the dye concentration to determine its influence on the measured diffusion coefficients, others have shown no measurable effect below concentrations of ~0.5 wt % in a variety of polymer/dye systems.[26,27,43] Therefore, these concentrations are believed to be sufficiently low that the tracer diffusion coefficient is indeed obtained.

Homogeneity of CO_2 in the sample is also required. To facilitate CO_2 equilibration, a thin polymer film with maximum exposed surface area is desirable, in order to minimize the length scale for CO_2 diffusion. However, a sufficient sample thickness is needed to ensure an adequate FRS signal. Both objectives are satisfied using a ~0.5 mm thick film, made by pressing the polymer/dye powder in a press mold and heating above T_g.[44] The resulting disk fits into the internal volume of the cell, and is transparent, homogeneous, inclusion-free, and nondistorting.

The assembled cell was allowed to equilibrate to the desired temperature and CO_2 pressure for at least 24 h before the first measurements. An equivalent equilibration time was allowed after any subsequent change in operating conditions to ensure an equilibrium CO_2 concentration throughout the sample. All experiments were carried out in the dark to eliminate the effect of stray light on the azobenzene photochemistry and to reduce background signals. A new location in the sample was chosen for each experiment. A single temperature (35 °C) and two grating spacings (1.20 and 0.87 μm) were studied. For the first grating spacing (1.20 μm), consecutive measurements were made as a function of increasing CO_2 pressure, *i.e.*, following an initial gas sorption isotherm. After reaching the maximum CO_2 pressure, the apparatus was realigned to obtain the second grating spacing (0.87 μm), and the CO_2 pressure decreased for subsequent measurements, *i.e.*, following a desorption isotherm.

For the FRS experiments carried out on PS-1K, azobenzene was combined with the oligomer in a 2 mm path length quartz cuvette (Hellma Cells), resulting in a final concentration of 0.2 wt %. The cell was sealed and the dye homogeneously mixed into the low-viscosity liquid oligomer at 70 °C. During FRS runs, a stainless steel holder for the cuvette provided temperature control via a circulating fluid from a constant-temperature bath. Several hours of equilibration were allowed between measurements after a change in temperature. For measurements below the glass transition temperature, no attempt was made to return to the melt state and then quench into the glassy state. Instead, the sample was progressively cooled through and below the glass transition temperature. The polymer glass was thus aged to a greater extent at each, subsequently lower temperature. A similar FRS study of dye diffusion in polystyrene oligomer approached these measurements in another manner, annealing for some time in the glassy state at the lowest temperature studied and slowly increasing the temperature across the glass transition.[27] This method also involves aging effects. However, the two approaches yield nearly identical results at temperatures not too far below the glass transition temperature.

IV. Results

Pure Polystyrene Oligomer. An example of the data obtained for the PS-1K/azobenzene system is shown in Figure 2. The results are typical of the "decay−growth−decay" kinetics observed at all temperatures and were fit to eq 2 employing a standard nonlinear least-squares regression algorithm. Two steps were taken to minimize the number of fitting parameters. First, C_{coh} and C_{inc} were determined directly from the data using the baseline and the signal value at the minimum between the first decay and subsequent growth. Second, the ratio of pre-exponential factors, A_1/A_2 (subscripts 1 and 2 are assigned to *trans*- and *cis*-azobenzene, respectively), was set to 1.20 based on an estimate of the relative optical contrast for *trans*- and *cis*-azobenzene concentration gratings in the PS oligomer (see Appendix). Note that the conditions required for decay−growth−decay kinetics (*i.e.*, if $A_1 > A_2$, then $\tau_1 < \tau_2$) identify the slower diffusing isomer as the *cis* isomer, which is consistent with results from previous studies of azo dye diffusion in bulk polymers,[40] polymer solutions,[45] and organic liquids.[46] The fit of A_2, τ_1, and τ_2 provides a robust, unique set of parameters to describe each decay−growth−decay signal. This approach avoids the problem of finding multiple parameter sets that fit the data equally well, a situation typically encountered when near-complete interference exists between the two diffracted optical fields.[26,33,47,48]

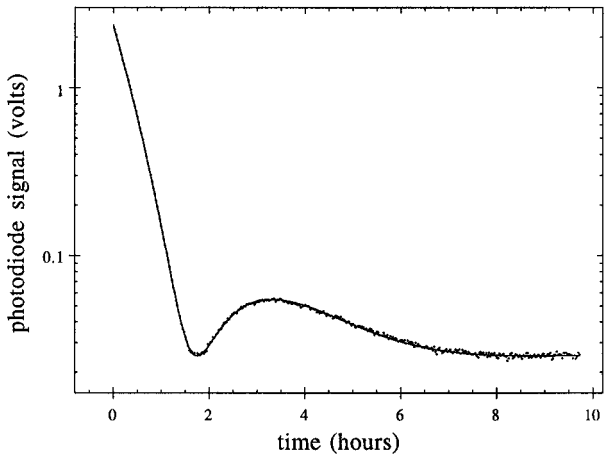

Figure 2. FRS result for PS-1K at 25 °C (=T_g + 10 °C) and d = 4.64 μm. The writing pulse occurs at t = 0. The points represent the recorded signal *vs* time, and the line through the points is a fit to eq 2: $A_1/A_2 \equiv 1.20$, $\tau_2/\tau_1 = 1.20$, $\tau_{avg} = 6010$ s (1.67 h).

The sensitivity of our analysis was examined by varying the value for A_1/A_2 imposed in the fitting process. As a result, the ratio τ_2/τ_1 was found to be well correlated with A_1/A_2 in the range $1.02 < A_1/A_2 < 2$, although all fits gave essentially equivalent representations of the data. In contrast, fits with $A_1/A_2 > 2$ exhibited obvious systematic deviations from the data, revealing a limit to the parameter values that could describe the relaxation kinetics. It was also found that the *average* relaxation time from the different successful fits was insensitive to the value of A_1/A_2; *i.e.*, $\tau_{avg} = (\tau_1 + \tau_2)/2$ remained constant to within 1%, even though the individual relaxation times varied by as much as 50%. Consequently, we use only this average relaxation time to characterize azobenzene diffusion in PS-1K. The same approach has been used previously to determine a single characteristic relaxation time from decay−growth−decay signals.[26,47,48] However, it is important to stress that assignment of an unambiguous value for each individual isomer relaxation time is indeed possible, after assigning a value to A_1/A_2. The accuracy of these relaxation times then depends on the accuracy to which the physical properties of the azobenzene isomers and polymer are known, since these values are needed to calculate A_1/A_2. We believe that $A_1/A_2 = 1.20$ offers a reliable estimate of the "true" value for this particular system.

The majority of experiments were repeated at several grating spacings for each temperature. The average diffusion coefficient D_{avg} was extracted from plots of $1/\tau_{avg}$ *vs* q^2; examples are shown in Figure 3. For all such plots, linear fits had near-zero intercepts, verifying that thermal reconversion made a negligible contribution to grating relaxation. For sub-T_g temperatures, where only one grating spacing was used, thermal

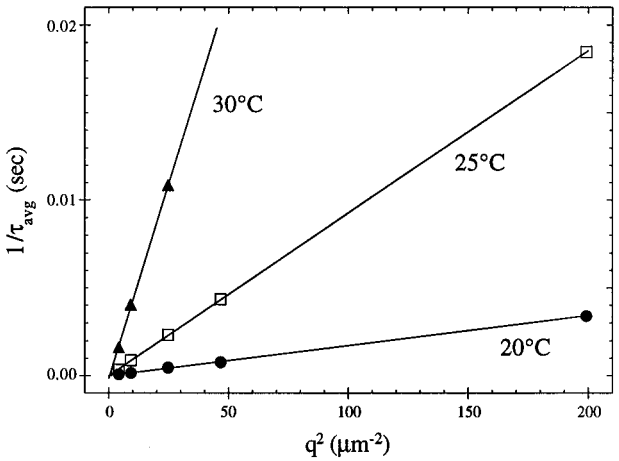

Figure 3. Inverse average relaxation time *vs* q^2 plots for PS-1K at 20, 25, and 30 °C. The linear fit for each temperature yields D_{avg} from the slope and τ_r from the intercept (found to be negligible in each case).

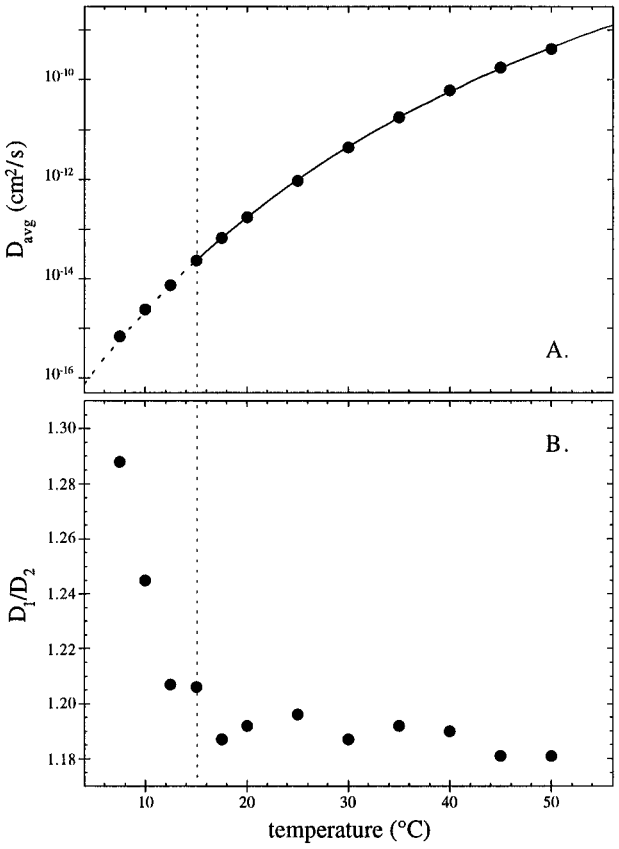

Figure 4. (A) Average azobenzene diffusion coefficient in PS-1K as a function of temperature. (—) WLF equation (eq 5) fit of $T > T_g$ data: $C_{1g} = 12.42$, $C_{2g} = 66.05$, log $D(T_g) = -13.64$; (- - -) extrapolation below T_g. (B) Ratio of diffusion coefficients for *trans*-(1) and *cis*-azobenzene (2) from fits with $A_1/A_2 \equiv 1.20$. The dotted line indicates T_g (=15 °C).

reconversion was assumed to be negligible in order to calculate D_{avg}. The temperature dependence of D_{avg} is shown in Figure 4A, and that of τ_2/τ_1 (= D_{trans}/D_{cis}) in Figure 4B. The latter plot shows the mobility of the *trans* isomer relative to the *cis* isomer remains nearly constant for $T > T_g$, but increases dramatically with decreasing temperature just below T_g.

In addition to decay−growth−decay kinetics, a second relaxation process was observed, apparently unrelated to translational diffusion of the dye molecules. This relaxation is manifested in an initial, fast decay of the

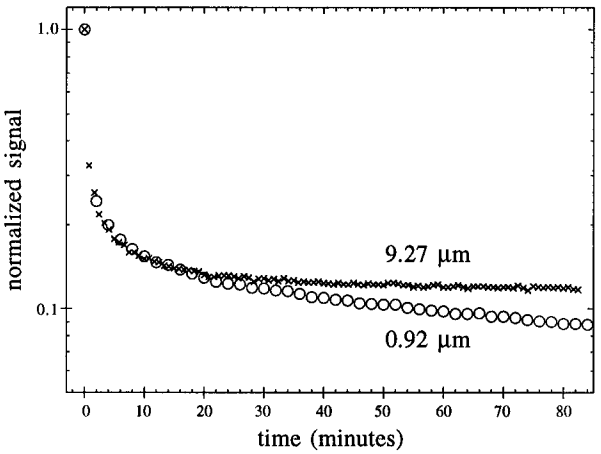

Figure 5. Initial relaxation behavior observed in PS-1K at 10 °C (T_g − 5 °C) for two grating spacings that differ by an order of magnitude. Identical decay kinetics are observed up to the onset of the decay−growth−decay process at ~20 min; subsequent deviation is due to the q^2 dependence of decay−growth−decay kinetics. The normalized signal is $S(t)/S(0)$, where $t = 0$ marks the end of the writing pulse. For each data set, the writing and reading beam polarizations were parallel, and the normalized pre-writing pulse baseline was on the order of 10^{-3}.

diffracted intensity immediately following the writing pulse and was observed on a time scale much shorter than for the subsequent decay−growth−decay process. The time scale for this decay depends strongly on temperature, decreasing by roughly an order of magnitude for every 5 °C increase in temperature near the glass transition. At 20 °C into the melt, the relaxation becomes too fast to observe. In addition, the rate of decay appears to be independent of grating spacing, even for spacings that differ by more than an order of magnitude, as shown in Figure 5. The time scale for this decay is too large to be attributed to thermal gradients induced by the writing process. Temperature gradients relax on a time scale of <100 μs for the length scales studied here, given that thermal diffusion coefficients are usually on the order of 10^{-3}−10^{-4} cm^2/s.[49] Moreover, the lack of q^2 scaling eliminates the possibility that this relaxation can be diffusive. A similar initial fast relaxation was reported for FRS signals from a thioindigo dye in several glassy polymers, but the origin of this behavior was not identified.[27]

It is likely that this initial relaxation is due to rotational diffusion of the azobenzene isomers, *i.e.*, to thermal randomization of nonuniform orientation distributions created by photoexcitation with polarized writing beams.[28,51,52] Since both isomers are anisotropic, their measured optical properties must depend on orientation. This causes the refractive index probed by the polarized reading beam to vary as the imposed orientation distributions relax, leading to a temporal variation in the total diffracted optical field. As only a local relaxation mechanism is involved, the kinetics should be independent of grating spacing, in agreement with the observed behavior. Results from a preliminary study of the effect of the relative writing and reading beam polarizations support this hypothesis. These results (Figure 6) qualitatively exhibit the signal kinetics expected for a rotational process when using parallel *vs* perpendicular writing-to-reading beam polarization geometries; that is, when one geometry yields a monotonic decay of the signal after the writing pulse, the other geometry should show a growth instead.[51] A quantitative analysis of the kinetics associated with

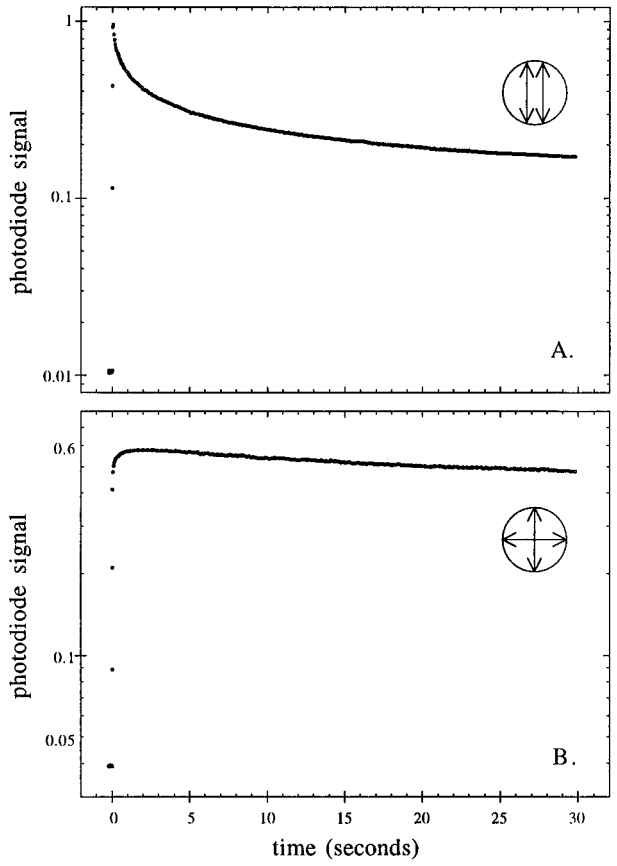

Figure 6. Initial relaxation behavior observed in PS-1K for two runs with different relative polarizations of the reading and writing beams: (A) parallel and (B) perpendicular. Conditions were otherwise identical: 15 °C (=T_g), $d = 4.64\ \mu$m, and 100 mW × 30 ms writing pulse beginning at $t = 0$. The characteristic time scale for decay−growth−decay kinetics, based on D_{avg} from Figure 4, is ~66 h at this temperature and grating spacing.

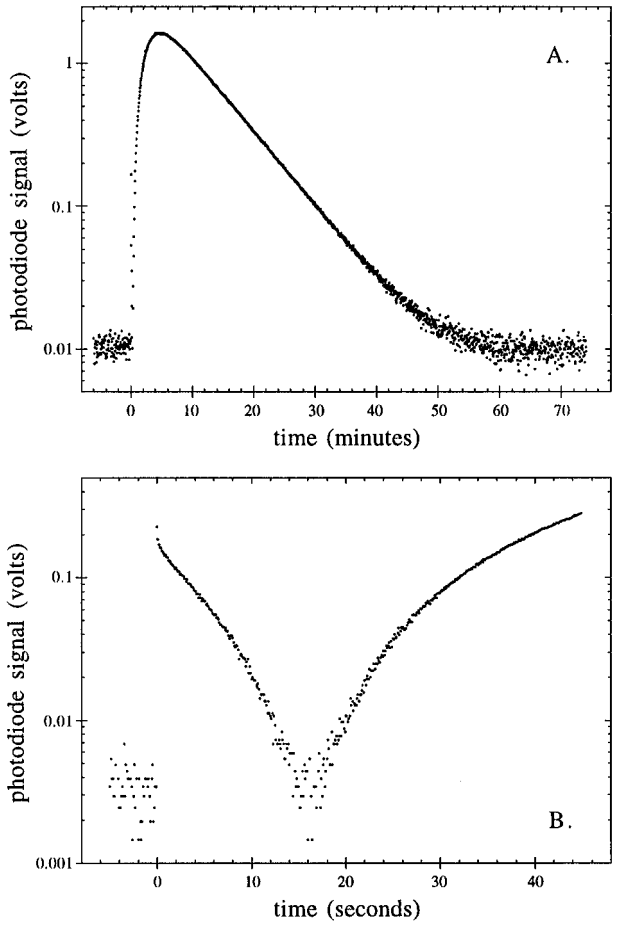

Figure 7. FRS results for the PS-36K/CO_2 system at 35 °C, $P_{CO_2} = 55$ bar, and $d = 1.20\ \mu$m. (A) Complete decay−growth−decay profile, which can be fit to eq 2: $A_1/A_2 = 1.11$, $\tau_2/\tau_1 = 10.1$, $\tau_2 = 1070$ s. (B) Initial decay behavior for a separate run under identical conditions, revealing the minimum associated with the decay−growth−decay kinetics and a fast relaxation process that occurs within the first 2 s after the writing pulse.

rotation of optically anisotropic probes is expected to be complicated, however, since both isomers contribute to the diffracted signal, have different optical anisotropies (in magnitude and orientation), and may have different rotational diffusivities. Such an analysis is beyond the scope of the present study.[53]

Polystyrene/CO_2 System. An example of the diffracted signal intensity *vs* time data obtained for azobenzene in the PS-36K polymer plasticized by CO_2 is shown in Figure 7. Decay−growth−decay kinetics are observed, as verified by the temporal behavior of the signal intensity at early times, shown in Figure 7B, where a decay to the baseline and subsequent growth can be clearly seen. An initial fast relaxation mode is also observed, similar to that seen in the PS-1K oligomer, leading to an inflection in the signal decay before the first minimum. Again, this contribution was more pronounced when the sample was well into the glassy region and decayed too rapidly to be observed as the polymer was further plasticized with CO_2. We attribute this initial relaxation to the same origin as that proposed for the oligomer (*i.e.*, rotational diffusion) and have made no attempt to study it explicitly.

Several characteristic features of the decay−growth−decay kinetics for this system are notably different from those observed for azobenzene in PS-1K and for other polymer/azo dye systems.[26,40,47,48,54] First, the initial minimum after the writing pulse occurs much earlier than the time required for the signal to completely relax. Second, the magnitude of the signal intensity achieved at the maximum (following the initial decay and subsequent growth) is much larger than that obtained immediately after the writing pulse. Finally, the signal decays nearly exponentially in time after the maximum. These features are consistent with a large difference in relaxation rates for the *cis* and *trans* isomer gratings.

The PS-36K/CO_2 data were fit to eq 2 in the same manner as the PS-1K data, with the exception that both A_1 and A_2 were allowed to vary independently. Assigning a constant value for A_1/A_2 was not necessary in this case, since the large difference in isomer relaxation times results in far less interference between the optical fields diffracted from the two isomer gratings. Thus, a unique parameter set could be identified for these experiments despite the additional degree of freedom associated with fitting A_1 and A_2 independently. In fact, the data could *not* be fit using $A_1/A_2 = 1.20$, due to systematic errors in describing the first decay−growth period of the signal.

For CO_2 pressures above 60 bar, an unexpected additional relaxation process was observed in the diffracted signal, which further complicated the data fitting. This relaxation is manifested as a second growth and subsequent decay following the primary decay−growth−decay period, as shown in Figure 8. The behavior is characterized by a time scale that exceeds

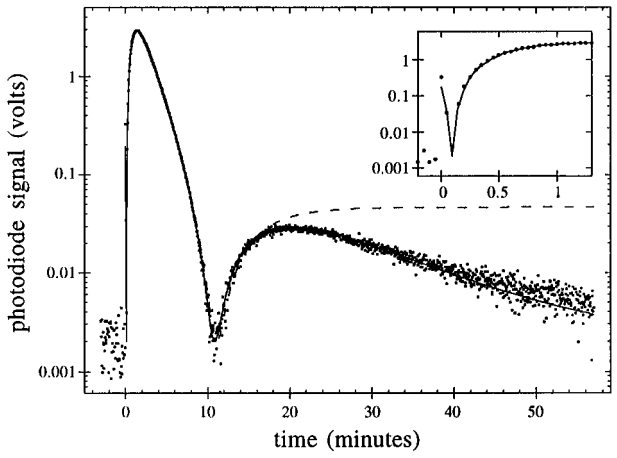

Figure 8. FRS result for the PS-36K/CO_2 system at 35 °C, $P_{CO_2} = 62$ bar, and $d = 1.20$ μm. (- - -) Fit to eq 2 using a large coherent scattering term: $A_1/A_2 = 1.07$, $\tau_1 = 34.8$ s, $\tau_2 = 249$ s, $C_1/C_2 = 6.8$; (—) Fit to eq 4: $A_1/A_2 = 0.98$, $A_1/A_3 = 6.64$, $\tau_1 = 34.1$ s, $\tau_2 = 274$ s, $\tau_3 = 1390$ s, $C_1 = 0$. The inset is a magnification of the initial relaxation behavior after the writing pulse, showing the first minimum at ~6 s.

decay−growth−decay kinetics by nearly an order of magnitude, with an eventual return to the original baseline. The signal intensity and the relaxation kinetics associated with this process varied systematically with pressure, becoming larger and decaying faster with increasing pressure. At the highest pressure studied, the maximum intensity reached ~10% of the highest value obtained during the decay−growth−decay process.

The presence of this relaxation required a new fitting approach. Two procedures were used. First, we discarded all points after the maximum created by the additional growth−decay process and fit the remaining data to eq 2 with five adjustable parameters (A_1, A_2, τ_1, τ_2, C_{coh}). In doing so, the effect of the long-time relaxation mode was incorporated entirely into C_{coh}. This procedure gives a satisfactory fit of the original decay−growth−decay kinetics but produces systematic deviations at longer times, as shown in Figure 8. As expected, the final relaxation cannot be described by a constant coherent scattering term, and the values obtained for C_{coh} are too large to be physically reasonable.

In the second procedure, we accounted for the long-time relaxation behavior explicitly by adding a third exponential relaxation term to the dual-grating model to describe the time dependence of the diffracted signal intensity:

$$I_d = \{A_1 e^{-t/\tau_1} - A_2 e^{-t/\tau_2} + A_3 e^{-t/\tau_3} + C_{coh}\}^2 + C_{inc}^2 \quad (4)$$

C_{coh} and C_{inc} were still determined from the baseline and signal minima, leaving six adjustable parameters. Fitting an entire data set using this equation accurately reproduces the second growth−decay kinetics, as shown by the solid line in Figure 8. The presence of an additional relaxation term implies that an additional grating is created by the writing process, which has the same spatial wavelength as the isomer gratings and contributes to the overall modulation in refractive index. The observed second growth−decay behavior is then a manifestation of this grating. A physical interpretation of the origin of this additional grating is given in the following section.

Table 1. Time Constant for the Relaxation Process Involved in the Second Growth−Decay Observed in PS-36K/CO_2 System (from Fits Using Eq 4)

grating spacing (μm)	P_{CO_2} (bar)	τ_3 (s)
1.20	62.1	1390
	63.4	848
	66.2	371
0.87	61.7	918
	84.8	12.7

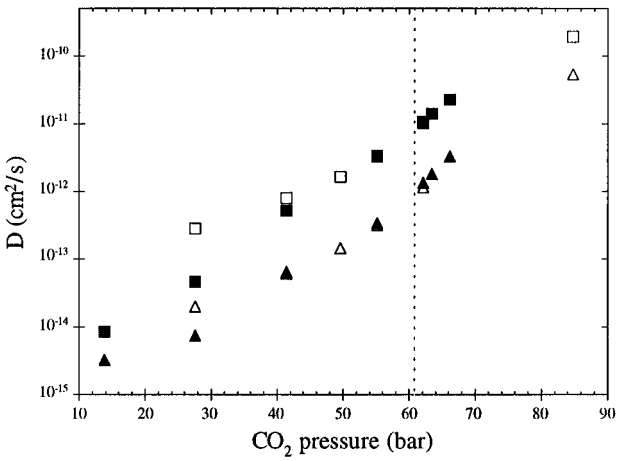

Figure 9. Diffusion coefficients for the two azobenzene isomers in the PS-36K/CO_2 system at 35 °C (from fits to eq 2 for $P_{CO_2} < 60$ bar, eq 4 for $P_{CO_2} > 60$ bar) under the assumption that the dye gratings relax only by diffusion. Results from both grating spacings are shown (1.20 μm: D_1 (■), D_2 (▲); 0.87 μm: D_1 (□), D_2 (△); 1 = *trans*, 2 = *cis*). The dotted line indicates the CO_2 pressure required to lower the system T_g to 35 °C.[18]

Using these two approaches, two sets of relaxation times were obtained for CO_2 pressures above 60 bar: one from the original dual-grating model (eq 2) and the other from the modified dual-grating model (eq 4). The faster relaxation time was nearly the same for the two models, differing by only ~10% at the highest CO_2 pressure, where the second growth−decay feature is most prominent. The difference was larger for the slower relaxation time, increasing from ~10% at 62 bar to ~50% at 85 bar. Invariably, the use of the modified dual-grating model reduced the faster and raised the slower relaxation times over the values obtained from the conventional dual−grating model. Values for τ_3, the time constant associated with the long-time (growth−decay) relaxation process, are given in Table 1.

The A_1/A_2 ratios from fits using eq 2 fell in the range of 1.06−1.16, in accord with our expectation that A_1 and A_2 should be similar. However, these ratio values are somewhat smaller than that calculated for azobenzene in pure polystyrene. It was also found that A_1/A_2 decreased with increasing CO_2 pressure. Both observations are consistent with the predicted effect of added CO_2 on the relative optical contrast of the two isomers in the polymer (see Appendix). The A_1/A_2 ratios from fits using eq 4 were close to or less than one and decreased with increasing CO_2 pressure as well. The A_1/A_3 ratios from these same fits were found to be much larger than one, decreasing from values of 6−8 to values of 3−4 with increasing pressure.

We have calculated diffusion coefficients using the relaxation times obtained from the two dual-grating models (eq 2 for $P_{CO_2} < 60$ bar and eq 4 for $P_{CO_2} > 60$ bar) by assuming negligible thermal reconversion. Results are presented in Figure 9. The assumption of negligible thermal reconversion is reasonable in light of our PS-1K results, which involve similar experimental

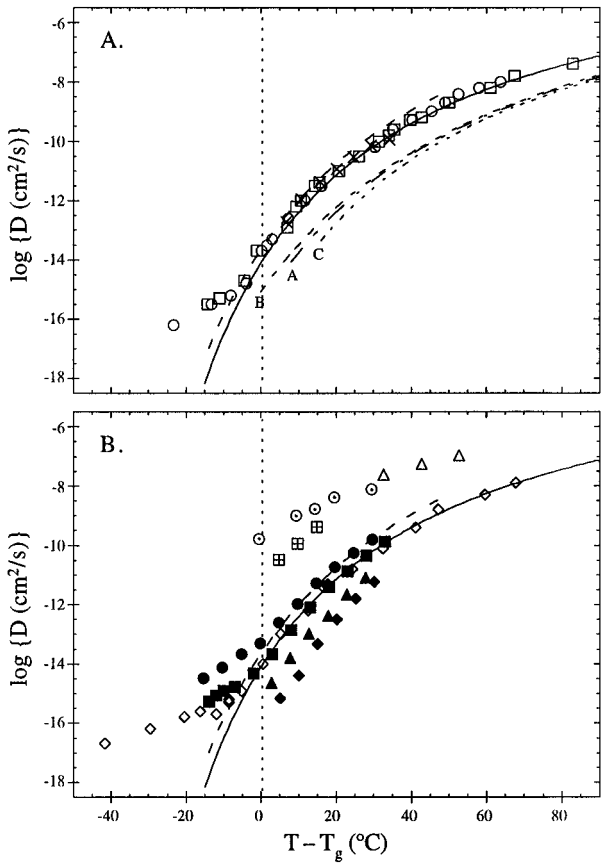

Figure 10. Diffusion coefficients of FRS probes in different polystyrene matrices: (A) pure PS; (B) PS with diluents. Symbols and lines are identified in Table 2.

time scales. In addition, for CO_2 pressures where time constants for two grating spacings are available, we verified the q^2 dependence of the relaxation times and evaluated directly the influence of thermal reconversion. The diffusion coefficients extracted in this manner agree well with those in Figure 9 at the highest pressures, where thermal reconversion is indeed found to make a negligible contribution to grating relaxation. Verification at lower pressures is more problematic due to CO_2 conditioning of the glassy polymer.[20−22] Since the 1.20 μm data were obtained for a sorption isotherm *before* CO_2 conditioning, while the 0.87 μm data were obtained for a desorption isotherm *after* conditioning, the two sets of time constants are expected to be increasingly unrelated at lower CO_2 pressures. This behavior is evident in Figure 9, where calculated diffusion coefficients are notably larger in the conditioned polymer than in the unconditioned polymer at the lowest pressures.

V. Discussion

Our results for azobenzene diffusion in the PS-1K are compared in Figure 10 with literature results for four other FRS probes in pure polystyrene of different molecular weights and in polystyrene/diluent matrices, as listed in Table 2. Glass transition temperatures range from 0 to 100 °C, and probe sizes relative to azobenzene range from 0.92 to 3.40. When temperature is scaled by the DSC-determined glass transition temperature for each pure PS matrix, the data in Figure 10A collapse onto essentially a single curve for $T > T_g$ for probes of similar size—azobenzene, TTI, and CQP—while the data for much larger cyclophane fall significantly below this curve. The diffusion coefficients for Aberchrome, which is almost identical in size to TTI, would then be expected to also fall on this curve. However, extrapolating the data for this dye in PS/toluene matrices (Figure 10B) to pure PS gives diffusion coefficients that actually lie far below the curve. It is thus apparent that these diffusion coefficients do not universally scale with probe size. Other factors must play a role, such as molecular shape and internal flexibility of the probe, and probe−matrix interactions. Results for the tracer-diffusion coefficients of tetracene and rubrene in PS measured by a holographic fluorescence recovery after photobleaching technique support this conclusion.[58] Figure 10B shows that the influence of added solvent is also not universal, since the enhancement in probe diffusivity when 10 wt % TCP is added to PS is accounted for by $(T - T_g)$ scaling while the effect of adding toluene at comparable concentrations is not.

Following standard practice, the temperature dependence of probe diffusion for $T > T_g$ is described by the Williams−Landel−Ferry (WLF) equation:[61]

$$\log D(T) = \log D(T_g) + \frac{C_{1g}(T - T_g)}{C_{2g} + (T - T_g)} \qquad (5)$$

The two WLF fits shown in Figure 10 provide a basis for comparison with our results for azobenzene diffusion in PS/CO_2: the solid line is the fit for TTI diffusion in high molecular weight polystyrene,[27] and the dashed line is the fit for azobenzene in the PS-1K oligomer from Figure 4A.

The observed behavior implies a common mechanism for probe diffusion at $T > T_g$, where Brownian motion of the probe is coupled to motions of the matrix.[27] Consequently, if changes in matrix dynamics occur simply as a result of changes in polymer chain motions, which are typically described using the time−temperature superposition principle for the pure polymer and concentrated polymer systems at hand, it should be possible to reconcile differences in probe diffusion by scaling the experimental temperature to a common reference temperature, such as T_g. The way in which this scaling depends on temperature, diluent concentration, or molecular weight is often described using free-volume concepts.[59,60] Specifically, the temperature dependence of free volume leads to the WLF equation. The result is that differences in probe mobility are accounted for simply by changes in the glass transition temperature of the host matrix. However, modestly different WLF parameters, and sometimes quite different log $D(T_g)$ values, are required for the different systems in Figure 10. It is obvious that the extent to which probe mobility and matrix dynamics are coupled, as well as the nature of the matrix dynamics involved, ultimately depends on the properties of the probe and any added diluent.

For $T < T_g$, despite fewer data spread over a more limited temperature range, the general trend is clearly toward a weaker temperature dependence than that given by the WLF equation, with deviations from WLF behavior beginning at or below T_g. This behavior suggests a change in the mechanism for probe diffusion. The temperature dependence has been described using an Arrhenius expression,[27,48] with apparent activation energies that increase with increasing T_g and fall in the range of 90−170 kJ/mol.[27] Continuation of WLF be-

Table 2. Key to Systems Plotted in Figure 10

symbol	matrix	T_g (°C)	FRS probe	[size[a]]	reference
– – –	PS-1K oligomer	15	azobenzene	[1.00]	Figure 4A
○, –	PS(M_w = 270 000)[b]	100	TTI[c]	[1.30]	27
□	PS 20-mer oligomer	66	TTI		27
×	PS(M_w = 244 000)	100	CQP[d]	[0.92]	55
– - –, A	PS(M_w = 422 000)	99	cyclophane	[3.40]	56
– – –, B	PS(M_w = 2800)	68	cyclophane		56
- - -, C	PS-d_8(M_w = 870)	24	cyclophane		56
◇	PS[e] + 10 wt % TCP[f]	69	TTI		27
●	PS[g] + 18.9 wt % toluene	0.3	Aberchrome	[1.29]	48
■	PS[g] + 16.0 wt % toluene	12.0	Aberchrome		48
▲	PS[g] + 13.6 wt % toluene	22.2	Aberchrome		48
◆	PS[g] + 11.9 wt % toluene	29.9	Aberchrome		48
△	PS[g] + 21.0 wt % toluene	7.7	azobenzene		48
⊙	PS[g] + 15.1 wt % toluene	15.6	azobenzene		48
⊞	PS[g] + 9.7 wt % toluene	40.2	azobenzene		48

[a] Molecular volume, relative to azobenzene, based on van der Waals volumes calculated using atomistic models.[57] [b] Solid line represents fit of $T > T_g$ data. [c] TTI = tetrahydrothiophene indigo dye. [d] CQP = camphorquinone dye photoproduct. [e] M_w = 270 000. [f] TCP = tricresyl phosphate. [g] M_w = 100 000.

havior below T_g can be attributed to physical aging, where extended annealing at sub-T_g temperatures allows structural relaxation to occur. Our own data for probe diffusion in PS-1K (Figure 4A) appear to follow WLF behavior over the entire temperature range studied, including slightly below T_g, which we attribute to the physical aging brought about by our experimental protocol; however, they do not extend far enough below T_g to determine if this behavior continues for $T \ll T_g$.

The results for azobenzene diffusion in PS plasticized by CO_2 can be compared to those in Figure 10 by mapping the CO_2 pressure axis in Figure 9 onto a ($T - T_g$) axis. A unique mapping is possible since each CO_2 pressure corresponds to a different T_g, and therefore to a different value for ($T - T_g$) at 35 °C. We calculate T_g as a function of P_{CO_2} at 35 °C using eq 6, derived from the measured CO_2 sorption isotherm[17] and the CO_2 concentration dependence of T_g,[18] both of which are approximately linear over the pressures of interest:

$$T_g(35°C, P_{CO_2}) = 101.1\ °C - (1.057\ °C/bar)P_{CO_2} \quad (6)$$

Glass transition temperatures thus calculated are believed to be accurate to roughly ±3 °C over a CO_2 pressure range of 0–60 bar; the uncertainty is somewhat larger in the 60–70 bar range. This expression predicts a CO_2 pressure of 62.5 bar is required to depress T_g to 35 °C, while the experimental value is 60.8 bar[18] (corresponding to a CO_2 concentration of ~8.5 wt %[17]). Equation 6 is not used to calculate T_g for P_{CO_2} > 70 bar due to uncertainties in extrapolating the measured sorption isotherm to higher pressures.

Using this mapping, we compare azobenzene diffusion in PS-36K/CO_2 to probe diffusion in other polystyrene matrices in Figure 11. Included in this comparison are the WLF fits from Figure 10, as well as the data for TTI in pure PS and in PS plasticized with TCP[27] and selected data for azobenzene in PS plasticized with toluene.[48] As discussed above, the diffusivities of azobenzene and TTI in the pure PS systems collapse onto essentially a single curve when plotted as a function of ($T - T_g$) over a range that includes the glass transition. Based on this observation, we assert that azobenzene and TTI diffusion will be similar in any pure PS matrix, both above and below the glass transition. The same also seems to apply to diffusion of these dyes in PS plasticized with TCP. Since the azobenzene diffusion coefficients in PS-36K/CO_2 are much greater, we conclude that for $T \leq T_g$, azobenzene diffusion in PS is

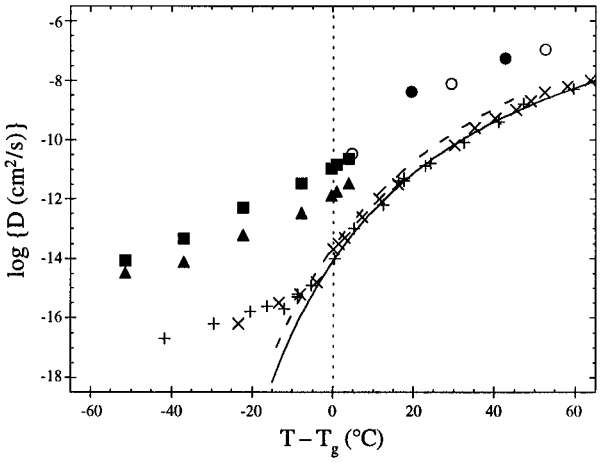

Figure 11. Diffusion coefficients for azobenzene isomers (D_{trans} (■), D_{cis} (▲)) in the PS-36K/CO_2 system from Figure 9, plotted as a function of the difference between 35 °C and T_g-(35 °C, P_{CO_2}); only the sorption isotherm data (d = 1.20 μm, P_{CO_2} < 70 bar) are shown. Data for azobenzene diffusion in PS/toluene solutions[48] from Figure 10 are also plotted as a function of $T - T_g$, where T = 35 (●) or 45 °C (○) and T_g varies with toluene concentration. The curves and other symbols represent WLF equation fits and data, respectively, from Figure 10: TTI in PS (–, ×) and in PS/10 wt % TCP (+); azobenzene in PS-1K (- - -).

substantially enhanced by the presence of CO_2. The enhancement is 2–3 orders of magnitude at $T = T_g$, and is maintained down to the lowest value of ($T - T_g$) studied, approximately −50 °C. Slightly above T_g, the effect is reduced by roughly an order of magnitude, perhaps due to the strong WLF ($T - T_g$) dependence of the diffusivity in the pure PS matrices.

In addition, the ($T - T_g$) dependence in the glass reveals that the rate of change in probe diffusivity obtained by depressing T_g with added CO_2 is similar to that obtained by increasing temperature at constant T_g, which has an apparent Arrhenius temperature dependence.[27] This behavior is surprising since, in one case, the ($T - T_g$) dependence of probe diffusion is related to the dilution and T_g-depression effects due to added CO_2, while in the other case, the ($T - T_g$) dependence involves processes that appear to be thermally activated.

At CO_2 pressures lower than those studied here, we expect probe diffusion in PS/CO_2 to exhibit a stronger dependence on ($T - T_g$). This follows because diffusivities in PS/CO_2 extrapolated to the unplasticized polymer at P_{CO_2} = 0 will be at least 2–3 orders of magnitude

greater than diffusivities extrapolated from the Arrhenius temperature dependence of the pure PS data. Therefore, the initial addition of CO_2 to unplasticized polystyrene would result in a rapid increase in probe mobility. Such an initial enhancement in mobility is not anticipated from the smooth, near-linear depression of T_g with CO_2 pressure, which suggests that the plasticization effect is a gradual one.[18,19] This hypothesis is supported, however, by results from NMR studies on the effect of CO_2 on glassy polymers, which demonstrate that local chain motions are enhanced significantly by the addition of small amounts of CO_2,[61] and that this enhancement quickly saturates at higher CO_2 pressures.[62]

Also included in our comparison are data for azobenzene in PS plasticized with toluene from Figure 10, which we have replotted on an equivalent basis, that is, as a function of $(T - T_g)$, holding temperature constant and varying T_g by changing toluene concentration. The data at 45 °C are included to aid in extrapolating the two data points at 35 °C to near the glass transition, where the $(T - T_g)$ range of the two PS/diluent data sets then nearly overlap. Similar enhancements in azobenzene diffusivities are obtained for the same value of $(T - T_g)$ for both PS/diluent systems. The diluent concentrations under these conditions are also approximately the same: ~10 wt % CO_2 or toluene. We conclude that CO_2 and toluene are comparable in terms of their ability to enhance the diffusion of azobenzene in PS, although CO_2 is slightly more efficient at depressing the glass transition.[18]

Note also that the enhanced diffusivity observed below T_g for PS/CO_2 is maintained above T_g for PS/toluene. Indeed, we expect azobenzene diffusion in PS/CO_2 and PS/toluene to show quantitatively similar behavior for $T > T_g$. However, the PS/CO_2 data will not extend much farther into the melt region, since the extent of CO_2-induced T_g depression is limited by the incremental increase in CO_2 solubility that can be achieved with increasing pressure above the critical pressure of CO_2. In fact, at CO_2 pressures greater than ~200 bar, the effect of hydrostatic pressure on T_g dominates the plasticization effect, causing T_g to increase with CO_2 pressure.[14] This limitation excludes the possibility that the isothermal PS/CO_2 data would follow a WLF dependence for $T \gg T_g$.

It is evident from the results in Figure 11 that the CO_2-induced glass transition depression alone does not account for the observed diffusivity enhancements. While this can also be said of the plasticization effect of toluene, it is in contrast with the behavior observed when TCP is used as the diluent. An additional mechanism, not directly embodied in the effects of the glass transition, must be important. One possibility is a decrease in the matrix density brought about by swelling of the polymer, as occurs with added toluene. Intuitively, this effect would result in increased probe mobilities. However, the experimental CO_2 sorption and swelling data[17] reveal that the overall density actually *increases* slightly with the addition of CO_2 in the 0−60 bar range. Notably, the addition of TCP should also increase the matrix density.

Within the context of a free-volume description of diffusion, the enhanced probe mobility in PS/CO_2 is due to more free volume in this matrix than in the other matrices at the same T_g-scaled temperature. This result is consistent with the notion that the glass transition is not an iso-free-volume state for diffusion. However, the application of free-volume theory to our system requires a prediction of how much free volume accompanies CO_2 upon sorption into the glassy polymer. Our calculations show that obtaining the measured enhancements would require treating virtually all the volume occupied by CO_2 as effective free volume. In addition, probe size is not the only factor in determining probe mobility in this system. Probe−matrix interactions, and perhaps shape effects, are quite important, and must be accounted for, particularly in interpreting the difference between the mobilities of *cis*- and *trans*-azobenzene.

Alternatively, the diffusivity enhancements can be interpreted in terms of local friction. We define a friction factor ζ_p for probe diffusion, which is related to an effective local matrix viscosity (or microviscosity) η_m through a generalized Stokes−Einstein relation:

$$D_{probe} = kT/\zeta_p = kT/(f_p \eta_m r_p) \tag{7}$$

The radius r_p is a measure of probe size, and f_p formally accounts for hydrodynamic boundary conditions and probe shape.[63] In a more general sense, f_p characterizes how effectively the matrix microviscosity generates a friction for a particular probe and should depend on both the probe and the matrix.[27] The relationships required to predict how η_m scales as a function of temperature and composition are the subject of current research.[64−67]

Within this framework, the enhanced diffusivity in PS/CO_2 must be due to a reduction in the friction experienced by the probe in the CO_2-plasticized matrix, relative to that in the pure PS matrix, even after accounting for the change in T_g. This effect could be attributed to simply the low viscosity of CO_2 (on the order of 10^{-2} cP at these conditions), or perhaps to the high mobility of CO_2 molecules. At issue is whether the addition of CO_2 primarily alters η_m or the extent of coupling between probe mobility and matrix dynamics embodied in f_p. Comparing plasticization by CO_2, toluene, and TCP provides some insight. In the absence of strong probe−diluent interactions, we can reasonably assume that f_p remains constant with the addition of diluent. The difference in behavior observed for CO_2 and toluene compared to that for TCP then occurs only due to differences in η_m: the presence of either CO_2 or toluene reduces η_m, while TCP appears to have no effect. Such a conclusion is intuitively consistent with the smaller molecular size and viscosity of CO_2 or toluene relative to TCP, which should itself be more strongly coupled to the slow dynamics of the polymer chains.[68] Also relevant to this issue is a recent suggestion that spatial heterogeneity in local polymer dynamics plays an important role in determining probe translation and rotation near T_g,[58] in that different diluents could potentially influence this spatial heterogeneity in substantially different ways. From this friction-based point of view, such an effect would further complicate prediction of an appropriate value for η_m.

If significant probe−diluent interactions exist, then probe−matrix coupling must also be considered. We believe this is the case in comparing the diffusivities for *cis*- and *trans*-azobenzene in PS/CO_2, which are shown to be different by roughly an order of magnitude in Figure 11. The difference is much larger than the 20−30% difference observed in PS-1K for $T \leq T_g$ and is

even quite large on the scale established by the overall CO_2 enhancement in probe diffusivity. Although the results in Figure 4B suggest that an increased difference in isomer mobility should be expected in the glass, a comparison of the behavior for these two systems at $T = T_g$ eliminates the possibility that this difference is due simply to the intrinsic properties of the isomers, independent of the matrix. Instead, we attribute it to a difference in isomer−matrix interactions, since intermolecular interactions between quadrupolar CO_2 molecules and the highly polar *cis* isomer of azobenzene ($\mu = 3.0$ D[69]) will be stronger than those between CO_2 and the nonpolar *trans* isomer. In this sense, the *trans* molecules are roughly equivalent in chemical nature to polystyrene segments, while the *cis* molecules act as preferential interaction sites for CO_2 due to their large dipole moments.

Two possible mechanisms involving the role of isomer−CO_2 interactions can be offered as the origin of the observed difference in isomer mobilities. The first is an increase in the effective size of a *cis* molecule, due to a physical association with CO_2, which reduces its mobility. Stokes−Einstein behavior will obviously fail to describe this difference.[27] However, if we consider the relationship between log D and solute size derived experimentally by Berens *et al.*[7] for solute diffusion in glassy poly(vinyl chloride), an order of magnitude difference in mobilities requires the effective radii to differ by only 0.1−0.2 Å, *i.e.*, ∼5% or less, or a volume difference of <20%. Free-volume theories of diffusion predict a similar strong size dependence.[60] Above T_g, the effect of size on log D is much weaker,[7] in line with the results in Figure 10**.** The second possible mechanism focuses instead on the probe friction factor: stronger interactions between the *cis* isomer and CO_2 lead to increased interactions with the PS/CO_2 matrix, in turn increasing the friction it experiences and reducing its mobility relative to the *trans* isomer. The end result in applying either mechanism is that preferential isomer−CO_2 interactions reduce the *cis* isomer mobility by increasing the overall coupling of its Brownian motion to the polymer/CO_2 matrix, relative to the same coupling for the *trans* isomer.

The difference in isomer polarity also plays an important role in our interpretation of the additional relaxation mode observed at long times in PS/CO_2 at high CO_2 pressures. Specifically, we assert the associated physical grating is a periodic perturbation in the spatial distribution of polymer chain segments and diluent molecules, induced by the *cis*-azobenzene concentration grating. This perturbation, though weak, contributes to the total modulation in refractive index. The thermodynamic driving force for this process is the difference in polarity between the two isomers, which leads to different interactions with the PS and CO_2 components of the host matrix.

The potential importance of specific interactions in FRS experiments has been emphasized in the literature. For example, consideration of probe−matrix interactions successfully accounted for large differences in the concentration dependence of probe diffusivities in hydrogen-bonding *vs* non-hydrogen-bonding polymer solutions.[47,54] Such interactions were also invoked to explain differences in isomer diffusivities in polymer melts[40] and organic liquids.[33] Most notably, the origin of nonexponential decays generated by spiropyran-labeled polymer chains in a Θ solvent were attributed to local modification of the solvent quality in the presence of the polar photoproduct, which produced a polymer concentration grating.[70]

If isomer-specific interactions exist, the isomer concentration gratings create a spatially modulated interaction field for PS and CO_2, which can be considered as a grating in chemical potential. This induces a physical grating in the matrix, involving a nonuniform *equilibrium* spatial distribution of the local densities of polymer chain segments and CO_2 molecules. The driving force associated with the Soret effect, where a temperature gradient induces a polymer concentration gradient, is conceptually similar.[71] Opposing this driving force is the tendency for the induced grating to relax to a uniform distribution by diffusion or by internal relaxation modes in the case of polymer chains. Eventually the matrix modulation must disappear, as the driving force vanishes when the isomer concentration gratings disappear. However, both polymer diffusion and large-scale internal relaxations occur on much slower time scales than dye diffusion, so that the time scale for this relaxation will be significantly greater than for decay−growth−decay. In fact, the apparent cutoff for this additional mode at a CO_2 pressure of 60 bar corresponds to the pressure required for a CO_2-induced glass transition in polystyrene at 35 °C.[18] Since the glass transition can be interpreted as the onset of substantial polymer chain mobility on the length scale probed by our experiment, this correspondence supports a matrix-related origin for the observed behavior.

We incorporate this matrix relaxation mechanism into the dual-grating model as follows. The matrix modulation, with amplitude Δm, occurs at the same grating wave vector as the isomer modulations. The instantaneous driving force for such a perturbation of the matrix is taken to be directly proportional to the instantaneous amplitudes of both isomer gratings. Relaxation is assumed to follow first-order kinetics, analogous to the dye concentration profiles which relax by diffusion. The time dependence of Δm is thus governed by

$$\frac{d\Delta m(t)}{dt} = -\frac{1}{\tau_m}[\Delta m(t) - (k_1\Delta c_1(t) + k_2\Delta c_2(t))] \quad (8)$$

where Δc_i is the amplitude of the concentration modulation for isomer i, k_i is a proportionality coefficient, and the time constant τ_m represents the rate of relaxation of the matrix modulation. The quantity in brackets is the deviation of the amplitude from its equilibrium value.

We next assume the driving force is dominated by the slower diffusing *cis* isomer, justified primarily by a time scale argument: the grating associated with the faster diffusing *trans* isomer disappears well before the appearance of the second growth−decay process. Furthermore, since the *cis* isomer is highly polar, and the *trans* isomer is nonpolar, a spatial variation in the isomer−matrix interaction strength is likely to be more important for the *cis* grating than the *trans* grating. Thus, $k_1\Delta c_1(t) \approx 0$. We also assume that isomer diffusion is not affected by the matrix modulation, and that thermal reconversion is negligible. The original expression for relaxation of the concentration grating amplitude (eq 1) can therefore be used for $\Delta c_2(t)$. With an initial condition that no matrix modulation exists immediately after the writing pulse (*i.e.*, $\Delta m(t=0) = 0$), the solution of eq 8 is

$$\Delta m(t) = \Delta m_0[e^{-t/\tau_m} - e^{-q^2D_2t}] \quad (9)$$

where

$$\Delta m_0 = k_2 \Delta c_0 / (\tau_m q^2 D_2 - 1) \quad (10)$$

The matrix modulation contributes to the overall modulation in the refractive index, so the time dependence for the diffracted intensity becomes

$$I_d = \{A_1 e^{-t/\tau_1} - A_2 e^{-t/\tau_2} + A_3[e^{-t/\tau_3} - e^{-t/\tau_2}] + C_{coh}\}^2 + C_{inc}^2 \quad (11)$$

where A_3 represents the magnitude of this contribution to the total diffracted optical field, and $\tau_3 = \tau_m$ is the time constant for its relaxation. This expression can be simplified to the form of eq 4, but the *apparent* A_2 parameter in that equation is equivalent to $(A_2 + A_3)$ in eq 11, revealing why values for A_1/A_2 obtained from fits using eq 4 were found to be less than unity. The same fits using eq 11 result in A_1/A_2 values greater than one, correctly representing the relative refractive indices of *trans*- and *cis*-azobenzene.

The proposed model is consistent with several important characteristics of this system. First, the additional relaxation is associated with motions of the polymer chains, based on the time scales observed in our experiments. Second, due to a large difference in mobilities, the *trans*-azobenzene concentration grating completely disappears before the *cis* concentration grating can relax to a significant extent, leaving a substantial spatial grating of polar *cis* isomer molecules in a roughly uniform background matrix of nonpolar molecules and CO_2. This unique condition, facilitated by the presence of CO_2, would likely induce a matrix response involving the polymer. Third, the polymer motions required for such a response are known to occur in CO_2-plasticized glassy polymers, even below T_g, as is evident from the experimentally observed effects of CO_2 conditioning, including hysteretic swelling and semi-permanent, unrelaxed volume dilation.[20−22] Lastly, we also note that dynamic light scattering investigations of concentrated polymer solutions near the glass transition reveal contributions to matrix dynamics from both concentration and density fluctuations.[72] These two modes, which are in general coupled, involve quite different relaxation mechanisms: concentration fluctuations relax by a q^2-dependent counter-diffusion process, while density fluctuations relax by q-independent local motions. Since these processes should also occur in PS/CO_2, it is reasonable to expect that either or both contribute to the overall relaxation behavior of the "forced fluctuation" imposed during the FRS experiment. Their relative contributions to our matrix relaxation mode could presumably be determined by studying its q dependence. Moreover, the molecular weight dependence for these two mechanisms is much different and could also be studied.

In closing, we comment on the apparent increase in probe diffusivity in CO_2-conditioned glassy polymer relative to unconditioned polymer at low CO_2 pressures demonstrated in Figure 9. The conditioning effect has been previously interpreted in terms of excess volume introduced during swelling that accompanies sorption of a plasticizing gas by a glassy polymer.[20−22] Upon depressurization, the sample is unable to completely relax to its original volume due to limited mobility of the constituent polymer chains.[61] In this context, probe diffusion is expected to increase after conditioning, due to the additional free volume in the system. The apparent increase in diffusivity exhibited in Figure 9, which approaches an order of magnitude at CO_2 pressures well below the glass transition pressure, is consistent with this mechanism; however, the magnitude of the effect is surprising.

VI. Conclusions

Our results show that the tracer diffusion of azobenzene in glassy PS is enhanced dramatically by the presence of CO_2. In this respect, plasticization by CO_2 increases dye diffusion in the same way as plasticization by adding liquid diluents, increasing temperature, or decreasing polymer molecular weight. However, the enhancement is roughly 2−3 orders of magnitude larger than that predicted on the basis of the diffusion of similar FRS dyes in pure PS and concentrated PS/TCP mixtures, for which dye mobility can be characterized almost exclusively by accounting for differences in T_g.

Due to this enhancement, the same diffusivity can be achieved in the glass at moderate temperatures in the presence of CO_2 as would be obtained in the pure polymer melt at much higher temperatures. For example, the azobenzene diffusivity at 35 °C and $P_{CO_2} =$ 50 bar is roughly equivalent to that expected at 110 °C in pure polystyrene. It is important to stress that this enhancement in diffusivity is not behavior exclusive to plasticization by CO_2. In fact, comparable dye diffusivity enhancements have also been observed with increasing concentrations of liquid toluene in PS.[48] However, CO_2 offers distinct advantages over liquid solvents, including its much higher diffusivities in glassy polymers[7] and unique solvent properties related to its supercritical fluid properties and its chemical nature.[1,2]

Our results also reveal that the extent of CO_2 enhancement for the *trans* isomer of azobenzene in the high molecular weight polymer is approximately an order of magnitude larger than that for the *cis* isomer. This selective enhancement in isomer mobilities is not as great in the pure PS-1K glass and therefore is also attributed to the presence of CO_2. The effect is presumably a manifestation of the large difference in isomer polarities, which leads to different intermolecular interactions with quadrupolar CO_2 and therefore the PS/CO_2 matrix.

Based on an extrapolation of our measurements to CO_2 pressures below 15 bar, we anticipate that the large enhancement in dye diffusivities in the glass is obtained with the initial addition of relatively small amounts of CO_2 at low pressures. After this initial enhancement, continued addition of CO_2 at constant temperature increases dye diffusivity to roughly the same extent as increasing $(T - T_g)$ in the pure PS glasses or those plasticized by liquid diluents. Notably, the addition of CO_2 at constant temperature is characterized by a near-linear dependence of log D on $(T - T_g)$ in this region.

Our studies have characterized two FRS relaxation processes in addition to decay−growth−decay kinetics associated with translational diffusion of the azobenzene isomers. The first process was observed as a fast initial relaxation occurring before dye translation and is attributed to rotation of the dye molecules. Since this process was observed in both the PS oligomer and the high molecular weight PS plasticized by CO_2, as well as in previous FRS studies on other polymers,[27] it is expected to be a generally observable FRS relaxation mode. The important implication of this finding is that rotation and translation of a single FRS probe can be studied for the same system under identical conditions.

However, to undertake this study first requires a rigorous quantitative analysis of rotational relaxation within the context of the FRS experiment.

The second additional relaxation process was observed only for CO_2-plasticized PS above the CO_2-induced glass transition. The dynamics were manifested in an additional growth and decay in the diffracted signal intensity that occurred only after the decay−growth−decay kinetics associated with dye diffusion. This behavior is attributed to the creation and relaxation of a periodic modulation in the spatial distribution of polymer segments induced by the presence of the *cis* isomer concentration grating. The effect of CO_2 plasticization, the large difference in dye isomer mobilities in the presence of CO_2, and interactions between the dye isomers and the PS/CO_2 matrix are thought to play important roles in this relaxation process. Additional experiments are clearly required to further characterize it. Indeed, examination of this relaxation process may offer a means of accessing polymer chain dynamics, without directly labeling the polymer. Such experiments would be novel in that they would probe slower dynamics and longer length scales than are accessible to conventional light scattering techniques.

The experimental results presented here have direct implications for molecular theories and engineering models that describe small-molecule diffusion in diluent-plasticized glassy polymers, in that they point to the importance of local matrix dynamics in determining solute mobility. The central issue is whether the presence of a plasticizer alters local motions to a different extent than the motions responsible for the glass transition, and if so, how such changes induced by CO_2 compare to the analogous changes brought about by temperature, liquid diluents, or chain ends. There is no reason to expect motions occurring on different time scales to respond identically to different means of plasticization, or even to plasticization by different diluents. Presumably, the effect of a particular form of plasticization on the sub-glass relaxations associated with local dynamics is central to the description of changes in solute diffusion. It would be interesting to probe these effects by studying solute mobility across sub-glass transitions induced by adding CO_2 *vs* other methods of plasticization. We have also seen that the mobility of probe molecules in a polymer matrix can be strongly influenced by specific solute−matrix interactions, including solute−diluent interactions. Based on these observations, we believe the most promising approach to interpreting probe diffusion within a molecular framework is to describe the local friction experienced by the probe molecule in terms of a coupling of probe motion to the dynamics of the polymer/diluent matrix.

Acknowledgment. Numerous helpful discussions with Prof. G. Astarita and technical assistance provided by G. Miller are gratefully acknowledged. This work was partially supported by a National Science Foundation Graduate Research Fellowship.

Appendix

In the general description of a phase-grating FRS experiment, both dye isomers contribute to the modulation in refractive index. Here we estimate the *ratio* of these contributions by using a generic expression for the refractive index of a dye/matrix mixture to relate the net refractive index grating to the isomer concentration gratings. This relationship allows us to specify the *relative* isomer contributions to the diffracted signal in terms of known physical properties of the dye and the matrix. Finally, we apply the model to azobenzene in polystyrene.

Starting with the Lorentz−Lorenz equation, it can be shown that the refractive index of the mixture in a typical FRS experiment is given by[73]

$$n = n_0 + \frac{(n_0^2 + 2)^2}{6n_0}\left\{\phi_1\left(\frac{R_1}{\bar{v}_1} - \frac{R_0}{\bar{v}_0}\right) + \phi_2\left(\frac{R_2}{\bar{v}_2} - \frac{R_0}{\bar{v}_0}\right)\right\} \tag{A1}$$

where n is refractive index, R is molar refractivity (related to the molecular polarizability), ϕ is volume fraction, and $\bar{v}$ is partial molar volume. Subscripts 0, 1, and 2 denote the background matrix, the original dye isomer, and the photoproduct dye isomer, respectively. Derivation of this equation assumes the dye is present at low concentration.

Equation A1 shows that the contribution from each dye isomer is a volume fraction weighted perturbation to the refractive index of the background matrix. It also gives the condition for which one isomer produces *no* change in the refractive index, *i.e.*, when one isomer is "index matched" to the background matrix. In general, this requires

$$\frac{R_i}{\bar{v}_i} = \frac{R_0}{\bar{v}_0} \tag{A2}$$

which can be reduced to $n_i = n_0$ if $\bar{v}_i$ and $\bar{v}_0$ are equal to their pure-component molar volumes.[73] Therefore, the typical index-matching criterion of $n_i = n_0$ applies only when the system forms an ideal mixture, but becomes a poor approximation when component i is dissolved in a highly compressible fluid at infinite dilution or when specific intermolecular interactions cause large solution nonidealities.

For the phase-grating FRS experiment, we are only concerned with the *modulation* in refractive index caused by the isomer concentration gratings. By defining a molar concentration c_i and making the substitution $\phi_i = c_i\bar{v}_i$, we can use eq 1 for the relaxation of each isomer grating to obtain an expression for the decay of the refractive index grating amplitude, $\Delta n(t)$:

$$\Delta n(t) = \frac{(n_0^2 + 2)^2}{6n_0}\left\{\Delta c_0 e^{-q^2 D_1 t}\left[\bar{v}_1\left(\frac{R_1}{\bar{v}_1} - \frac{R_0}{\bar{v}_0}\right)\right] - \Delta c_0 e^{-q^2 D_2 t}\left[\bar{v}_2\left(\frac{R_2}{\bar{v}_2} - \frac{R_0}{\bar{v}_0}\right)\right]\right\} \tag{A3}$$

where Δc_0 is the initial amplitude of both isomer concentration gratings, and the opposite sign of the two exponential terms arises due to the 180° phase difference between these gratings. It should be stressed that in using eq 1, we have assumed the rate of thermal reconversion is negligible. A more complicated expression and subsequent analysis will result if indeed this is not valid.

Substituting eq A3 into the relationship between the refractive index grating and diffracted intensity, $I_d \sim [\Delta n]^2$, produces the dual-grating model (*i.e.*, eq 2, neglecting the coherent and incoherent scattering contributions) with the constants A_1 and A_2 defined as appropriate collections of time-independent parameters. The ratio of these two constants is given by

$$\frac{A_1}{A_2} = \frac{\bar{v}_1\left(\frac{R_1}{\bar{v}_1} - \frac{R_0}{\bar{v}_0}\right)}{\bar{v}_2\left(\frac{R_2}{\bar{v}_2} - \frac{R_0}{\bar{v}_0}\right)} \tag{A4}$$

Replacing the partial molar volume of each component by its pure-component molar volume simplifies this expression to one involving only pure-component properties:

$$\frac{A_1}{A_2} = \frac{v_1}{v_2}\left\{\frac{f(n_1) - f(n_0)}{f(n_2) - f(n_0)}\right\} \tag{A5}$$

where the function f(n) represents the Lorentz−Lorenz equation for a pure component:

$$f(n_i) = \frac{R_i}{v_i} = \frac{n_i^2 - 1}{n_i^2 + 2} \tag{A6}$$

We now apply eq A5 to azobenzene in pure polystyrene. Relevant physical properties and calculated quantities are listed in Table 3. The ratio of refractive index grating amplitudes (*i.e.*, A_1/A_2) for complementary *trans*- and *cis*-azobenzene concentration gratings is determined to be 1.21 in high molecular weight PS and 1.20 in PS oligomer. This value is not expected to be a strong function of temperature, since the temperature dependence of the molar volumes of the dye and polymer should be similar and the molar refractivity is taken to be independent of temperature. The value for A_1/A_2 should also apply at our reading beam wavelength (633 nm), since the wavelength dependence of the dye and polymer molar refractivities should be similar in this wavelength region.

Note the consequence of making the first-order approximation[37] that the contribution to the refractive index by each isomer is proportional to $(n_i - n_0)$ instead of $v_i\{f(n_i) - f(n_0)\}$. For the PS oligomer/azobenzene system, the ratio of contributions would be 1.14 if calculated using $A_1/A_2 = (n_1 - n_0)/(n_2 - n_0)$, which amounts to a 30% smaller prediction for the relative optical contrast of the *trans* and *cis* refractive index gratings. This smaller value is essentially the same as that determined using eq A5 if $v_1 = v_2$. In fact, such agreement is expected whenever $f(n_i)$ for both isomers can be well represented by a truncated series expansion about $n = n_0$. However, $v_1 = v_2$ does not always hold, and even small differences between v_1 and v_2 (as for azobenzene; see Table 3) can change A_1/A_2 significantly.

To predict how addition of CO_2 should change A_1/A_2, we treat the background matrix as a homogeneous mixture of CO_2 in polystyrene and calculate a new value for $f(n_0)$ to be used in eq A5. For CO_2, we calculate a molar refractivity of 6.835 cm^3/mol using a group additivity method,[74] and a partial molar volume of 34.6 cm^3/mol obtained from sorption and swelling data for CO_2 in polystyrene at 35°C and $P_{CO_2} < 60$ bar.[17] The new value for $f(n_0)$ is obtained by applying the Lorentz-Lorenz equation to just the PS/CO_2 mixture, with polystyrene treated on a "per-mer" basis (see Table 3). Since $\bar{v}_{CO_2}/\bar{v}_{PSmer} > R_{CO_2}/R_{PSmer}$, $f(n_0)$ for this mixture will always be less than $f(n_0)$ for the pure polymer, and the addition of CO_2 brings A_1/A_2 closer to 1. For example, $A_1/A_2 = 1.17$ when the CO_2 concentration in high molecular weight PS reaches 5 wt %. Since the partial molar volume of CO_2 in the polymer is nearly independent of CO_2 pressure for $T < T_g(T,P_{CO_2})$, $f(n_0)$ should continue to decrease as the amount of CO_2 in the polymer increases. Correspondingly, the value for A_1/A_2 is predicted to decrease further with increasing CO_2 pressure. Beyond the CO_2-induced glass transition, the partial molar volume of CO_2 in PS increases rapidly, so that $f(n_0)$ and A_1/A_2 should then decrease even faster with increasing CO_2 pressure.

Table 3. Physical Properties for Polystyrene and Azobenzene

mixture component	refractive index[a]	$f(n_i)$	v_i (cm^3/mol)	R$_i$ (cm^3/mol)
high-M_w PS	1.591[b]	0.338	100[e]	33.8[g]
PS oligomer	1.585[c]	0.335	101[e]	33.8[g]
trans-azobenzene	1.700[d]	0.387	169[f]	65.2
cis-azobenzene	1.686[d]	0.380	163[f]	61.8

[a] Evaluated at the sodium D line wavelength (589.3 nm). [b] Average for glassy polystyrene, from ref 50, p VI/457. [c] At 20 °C. Experimentally determined using an Abbe refractometer. [d] Calculated from the composition dependence of the refractive index of *p*-xylene/azobenzene solutions at 20 °C (measured using an Abbe refractometer) and by assuming that the ratio of refractive indices for *trans*- to *cis*-azobenzene is equal to the same ratio for *trans*- to *cis*-stilbene,[37] which has an electronic structure nearly identical to that of azobenzene. The values for stilbene at 20 °C were obtained from ref 74: $n_{trans} = 1.6264$, $n_{cis} = 1.6130$. [e] On a "per-mer" basis, using a mer molecular weight of 104 g/mol and measured densities at 25 °C: 1.04 g/cm^3 for high-M_w polystyrene and 1.03 g/cm^3 for oligomer polystyrene.[75] [f] These values represent the partial molar volumes of *trans*- and *cis*-azobenzene in benzene at 25 °C, determined using data in ref 69. [g] On a "per-mer" basis. See ref 50, p VI/451.

References and Notes

(1) (a) Williams, D. F. *Chem. Eng. Sci.* **1981**, *36*, 1769. (b) Paulaitis, M. E.; Krukonis, V. J.; Kurnik, R. T.; Reid, R. C. *Rev. Chem. Eng.* **1983**, *1*, 179.
(2) McHugh, M. A.; Krukonis, V. J. *Supercritical Fluid Extraction: Theory and Applications*, 2nd Ed.; Butterworth-Heinemann: Boston, 1994.
(3) Burgess, A. N.; Jackson, K. *J. Appl. Polym. Sci.* **1992**, *46*, 1395.
(4) Dhalewadikar, S. V.; McHugh, M. A.; Guckes, T. L. *J. Appl. Polym. Sci.* **1987**, *33*, 521.
(5) Hirata, Y.; Okamoto, Y. *J. Microcolumn Sep.* **1989**, *1*, 46.
(6) *Supercritical Fluid Processing of Food and Biomaterials*; Rizvi, S. S. H., Ed.; Blackie Academic & Professional: London, 1994.
(7) Berens, A. R.; Huvard, G. S.; Korsmeyer, R. W.; Kunig, F. W. *J. Appl. Polym. Sci.* **1992**, *46*, 231.
(8) Tom, J. W.; Lim, G. B.; Debenedetti, P. G.; Prud'homme, R. K. In *Supercritical Fluid Engineering Science: Fundamentals and Applications*; Kiran, E., Brennecke, J. F., Eds.; American Chemical Society: Washington, DC, 1993.
(9) Howdle, S. M.; Ramsay, J. M.; Cooper, A. I. *J. Polym. Sci., Polym. Phys. Ed.* **1994**, *32*, 541.
(10) Romack, T. J.; Maury, E. E.; DeSimone, J. M. *Macromolecules* **1995**, *28*, 912 and references therein.
(11) (a) Adamsky, F. A.; Beckman, E. J. *Macromolecules* **1994**, *27*, 312. (b) Watkins, J. J.; McCarthy, T. J. *Macromolecules* **1994**, *27*, 4845.
(12) (a) Shim, J. J.; Johnston, K. P. *AIChE J.* **1989**, *35*, 1097. (b) Shim, J. J.; Johnston, K. P. *AIChE J.* **1991**, *37*, 607.
(13) Debenedetti, P. G.; Reid, R. C. *AIChE J.* **1986**, *32*, 2034.
(14) Wang, W. C.; Kramer, E. J.; Sachse, W. H. *J. Polym. Sci., Polym. Phys. Ed.* **1982**, *20*, 1371.
(15) Chiou, J. S.; Barlow, J. W.; Paul, D. R. *J. Appl. Polym. Sci.* **1985**, *30*, 2633.
(16) Berens, A. R.; Huvard, G. S. In *Supercritical Fluid Science and Technology*; Johnston, K. P., Penninger, J. M. L., Eds.; American Chemical Society: Washington, DC, 1989.
(17) Wissinger, R. G.; Paulaitis, M. E. *J. Polym. Sci., Polym. Phys. Ed.* **1987**, *25*, 2497.
(18) Wissinger, R. G.; Paulaitis, M. E. *J. Polym. Sci., Polym. Phys. Ed.* **1991**, *29*, 631.

(19) Condo, P. D.; Paul, D. R.; Johnston, K. P. *Macromolecules* **1994**, *27*, 365.
(20) Sefcik, M. D. *J. Polym. Sci., Polym. Phys. Ed.* **1986**, *24*, 957.
(21) (a) Kamiya, Y.; Hirose, T.; Mizoguchi, K.; Naito, Y. *J. Polym. Sci., Polym. Phys. Ed.* **1986**, *24*, 1525. (b) Kamiya, Y.; Hirose, T.; Mizoguchi, K.; Terada, K. *J. Polym. Sci., Polym. Phys. Ed.* **1988**, *26*, 1409.
(22) Fleming, G. K.; Koros, W. J. *Macromolecules* **1990**, *23*, 1353.
(23) Dooley, K. M.; Knopf, F. C.; Becnel, J.; Caines, A. In *Innovations in Supercritical Fluids: Science and Technology*; Hutchenson, K. W., Foster, N. R., Eds.; American Chemical Society, Washington, DC, 1995.
(24) Cotton, N. J.; Bartle, K. D.; Clifford, A. A.; Dowle, C. J. *J. Appl. Polym. Sci.* **1993**, *48*, 1607.
(25) Nealey, P. F.; Cohen, R. E.; Argon, A. S. *Macromolecules* **1994**, *27*, 4193.
(26) Huang, W. J.; Frick, T. S.; Landry, M. R.; Lee, J. A.; Lodge, T. P.; Tirrell, M. *AIChE J.* **1987**, *33*, 573.
(27) Ehlich, D.; Sillescu, H. *Macromolecules* **1990**, *23*, 1600.
(28) Rondelez, F. In *Light Scattering in Liquids and Macromolecular Solutions*; Degiorgio, V., Corti, M., Giglio, M., Eds.; Plenum: New York, 1980.
(29) Bräuchle, C.; Burland, D. M. *Angew. Chem., Int. Ed. Engl.* **1983**, *22*, 582.
(30) Eichler, H. J.; Günter, P.; Pohl, D. W. *Laser-Induced Dynamic Gratings*; Springer-Verlag: Berlin, 1986.
(31) Sillescu, H.; Ehlich, D. In *Lasers in Polymer Science and Technology*; Fouassier, J. P., Rabek, J. F., Eds.; CRC Press: Boca Raton, FL, 1990; Vol. III, Chapter 7.
(32) Miles, D. G.; Lamb, P. D.; Rhee, K. W.; Johnson, C. S., Jr. *J. Phys. Chem.* **1983**, *87*, 4815.
(33) Terazima, M.; Okamoto, K.; Hirota, N. *J. Phys. Chem.* **1993**, *97*, 5188.
(34) Kogelnik, H. *Bell Syst. Tech. J.* **1969**, *48*, 2909.
(35) Rhee, K. W.; Gabriel, D. A.; Johnson, C. S., Jr. *J. Phys. Chem.* **1984**, *88*, 4010.
(36) Wang, C. H.; Xia, J. L. *J. Chem. Phys.* **1990**, *92*, 2603.
(37) Park, S.; Sung, J.; Kim, H.; Chang, T. *J. Phys. Chem.* **1991**, *95*, 7121.
(38) Ross, D. L.; Blanc, J. In *Techniques of Chemistry: Photochromism*; Brown, G. H., Ed.; Wiley-Interscience: New York, 1971; Vol. III, Chapter 5.
(39) Landry, M. R.; Gu, Q.; Yu, H. *Macromolecules* **1988**, *21*, 1158.
(40) Lee, J.; Park, K.; Chang, T.; Jung, J. C. *Macromolecules* **1992**, *25*, 6977.
(41) Hartely, G. S. *J. Chem. Soc.* **1938**, 633.
(42) (a) Eisenbach, C. D. *Makromol. Chem.* **1978**, *179*, 2489. (b) Mita, I.; Horie, K.; Hirao, K. *Macromolecules* **1989**, *22*, 558.
(43) Zhang, X. Q.; Wang, C. H. *Macromolecules* **1990**, *23*, 1218.
(44) This sample preparation method was suggested by Prof. M. D. Ediger, University of Wisconsin (private communication).
(45) Lee, J.; Park, T.; Sung, J.; Park, S.; Chang, T. *Bull. Korean Chem. Soc.* **1991**, *12*, 569.
(46) Lever, L. S.; Bradley, M. S.; Johnson, C. S., Jr. *J. Magn. Reson.* **1986**, *68*, 335.
(47) (a) Lee, J. A.; Lodge, T. P. *J. Phys. Chem.* **1987**, *91*, 5546. (b) Lodge, T. P.; Lee, J. A.; Frick, T. S. *J. Polym. Sci., Polym. Phys. Ed.* **1990**, *28*, 2607.
(48) Frick, T. S.; Huang, W. J.; Tirrell, M.; Lodge, T. P. *J. Polym. Sci., Polym. Phys. Ed.* **1990**, *28*, 2629.
(49) Thermal diffusion coefficient = thermal conductivity/(density × specific heat capacity). Estimates of these physical properties for liquids (see Bird, R. B.; Stewart, W. E.; Lightfoot, E. N. *Transport Phenomena*; Wiley: New York, 1960) and polymers (see ref 50) yield values of 10^{-3}–10^{-4} cm^2/s for the thermal diffusion coefficient.
(50) *Polymer Handbook*, 3rd Ed.; Brandrup, J., Immergut, E. H., Eds.; Wiley: New York, 1989.
(51) Moog, R. S.; Ediger, M. D.; Boxer, S. G.; Fayer, M. D. *J. Phys. Chem.* **1982**, *86*, 4694.
(52) Hyde, P. D.; Ediger, M. D. *J. Chem. Phys.* **1990**, *92*, 1036.
(53) The analysis required is similar to that for rotation of anisotropic molecules within the theories of light scattering (Pecora, R.; Steele, W. A. *J. Chem. Phys.* **1965**, *42*, 1872), fluorescence depolarization (Chuang, T. J.; Eisenthal, K. B. *J. Chem. Phys.* **1972**, *57*, 5094), and the transient grating technique for amplitude gratings (von Jena, A.; Lessing, H. E. *Opt. Quantum Electron.* **1979**, *11*, 419).
(54) Xia, J. L.; Gong, S. S.; Wang, C. H. *J. Phys. Chem.* **1987**, *91*, 5805.
(55) Zhang, J.; Wang, C. H.; Chen, Z.-X. *J. Chem. Phys.* **1986**, *85*, 5359.
(56) Kim, H.; Waldow, D. A.; Han, C. C.; Tran-Cong, Q.; Yamamoto, M. *Polym. Commun.* **1991**, *32*, 108.
(57) Calculated using QUANTA 2.1 (Polygen Corp., Waltham, MA). Identical relative volumes are obtained from molar volumes at 0 K calculated using standard group contribution methods (Haward, R. N. *J. Macromol. Sci., Rev. Macromol. Chem.* **1970**, *C4*, 191).
(58) Cicerone, M. T.; Blackburn, F. R.; Ediger, M. D. *Macromolecules* **1995**, *28*, 8224.
(59) Ferry, J. D. *Viscoelastic Properties of Polymers*, 3rd Ed.; Wiley: New York, 1980.
(60) (a) Fujita, H. *Fortschr. Hochpolym. Forsch.* **1961**, *3*, 1. (b) Vrentas, J. S.; Duda, J. L. *J. Polym. Sci., Polym. Phys. Ed.* **1977**, *15*, 403, 417.
(61) Sefcik, M. D.; Schaefer, J. *J. Polym. Sci., Polym. Phys. Ed.* **1983**, *21*, 1055.
(62) Smith, P. B.; Moll, D. J. *Macromolecules* **1990**, *23*, 3250.
(63) Dote, J. L.; Kivelson, D.; Schwartz, R. N. *J. Phys. Chem.* **1981**, *85*, 2169.
(64) Lodge, T. P. *J. Phys. Chem.* **1993**, *97*, 1480.
(65) Gissler, D. J.; Johnson, B. S.; Ediger, M. D.; von Meerwall, E. D. *Macromolecules* **1993**, *26*, 512.
(66) Floudas, G.; Steffen, W.; Fischer, E. W.; Brown, W. *J. Chem. Phys.* **1993**, *99*, 695.
(67) Ngai, K. L.; Rizos, A. K. *Macromolecules* **1994**, *27*, 4493.
(68) The size of the diluent is not the only property involved in determining the change in matrix microviscosity. Internal flexibility, for example, should also play a role for large diluents. This may explain the enhanced diffusivity of CQP in PS plasticized by dioctyl phthalate near T_g (Zhang, J.; Wang, C. H. *Macromolecules* **1988**, *21*, 1811), which contrasts the behavior for TCP despite the similar size of the two molecules.
(69) Hartley, G. S.; Le Fèvre, R. J. W. *J. Chem. Soc.* **1939**, 531.
(70) Deschamps, H.; Leger, L. *Macromolecules* **1986**, *19*, 2760.
(71) Köhler, W. *J. Chem. Phys.* **1993**, *98*, 660.
(72) Konak, C.; Brown, W. *J. Chem. Phys.* **1993**, *98*, 9014.
(73) Chapman, B. R. Ph.D. Thesis, University of Delaware, Newark, DE, 1996.
(74) *Handbook of Chemistry and Physics*, 65th Ed.; Weast, R. C., Ed.; CRC Press: Boca Raton, FL, 1984.
(75) Experimental data from G. Dee, DuPont (personal communication).

MA951469V